Brain Tumor Segmentation and Volume Estimation from T1-Contrasted and T2 MRIs

Amrit Hanuman   *amrit2025@hotmail.com*
Manufacturing and Design Engineering,
The University of Trinidad and Tobago, San Fernando Campus,
San Fernando, Trinidad and Tobago

Ken Sooknanan   *ken.sooknanan@utt.edu.tt*
Information and Communications Technology,
The University of Trinidad and Tobago, John Donaldson Campus,
Port of Spain, Trinidad and Tobago

Abstract

Amid the variations of the cancer disease, brain tumors account for the majority deaths among young people. To diagnose and treat this deadly disease effectively, analysis of hundreds of medical images such as Magnetic Resonance Imaging (MRI) scans is usually performed. However, the analyses of these scans are still mainly performed manually, making the procedure not only very tedious and time-consuming for doctors, but also error prone and non-repeatable. Attempts have been made to automate this procedure by performing image processing techniques such as thresholding, region-growing, unsupervised learning (e.g. k-means, fuzzy c-means clustering), and supervised learning (e.g. support vector machines). Some require human interaction. The techniques may be applied on one or more MRI sequence scans. Unfortunately, these automated attempts still result in a high level of error, and more computationally complex algorithms do not guarantee an increase in accuracy. This paper presents a novel, fully automatic brain tumor segmentation and volume estimation method using simple techniques on T1-contrasted and T2 MRIs. This new approach implemented five main steps: preprocessing using anisotropic diffusion, segmentation of tumor regions using k-means clustering, region combination using logical and Morphological operations, error checking using temporal smoothing, and volumetric measurement. When compared with five state-of-the-art algorithms, the proposed algorithm outperformed those in past works. Advances were seen by its noise reduction, increase in accuracy and closeness to actual tumor volume.

Keywords: Brain Tumor, Magnetic Resonance Imaging (MRI), Segmentation, Volume Estimation.

1. INTRODUCTION

A tumor is a mass of tissue formed by the uncontrolled growth of abnormal cells. A brain tumor can directly destroy healthy brain cells or do so indirectly by crowding other parts of the brain and causing inflammation, swelling and pressure within the skull [1]. In medical image analysis, segmentation of brain tumors from the background of magnetic resonance images (MRI) is crucial for effective diagnosis, treatment and monitoring of the disease [2]. However, segmentation is still done manually producing results that vary from expert to expert [3]. It is a difficult task as tumors vary greatly in size, shape and location. Additionally, tumors may appear to overlap with healthy brain tissue having similar intensity levels, which makes it even more difficult to distinguish the two. This process is time-consuming, non-repeatable, and prone to human errors causing inaccurate diagnosis that may lead to the death of patients. Thus, there is a demand for more accurate, time-efficient, computer aided methods to delineate tumor boundaries [4, 5].

Cancer is among the leading causes of death worldwide, with 14.1 million new cases and 8.2 million deaths recorded in 2012. The World Health Organization [6] reports that new cancer cases are expected to rise to about 70% over the next two decades. Tumors are mainly classified as either malignant or benign. Malignant tumors are cancerous; they are life-threatening and can spread to other parts of the body. Benign tumors do not contain cancer cells; they are not harmful and do not spread to other body parts [3]. Tumors may also be described based on their place of origination. A primary brain tumor originates in the brain, whereas a metastatic brain tumor originates in another part of the body and spreads to the brain [7].

Medical imaging modalities used for diagnosis of tumors include MRI and Computerized Tomography (CT). MRI provides greater contrast between soft tissues [8], making it more effective for tumor detection and segmentation. Segmentation is defined as the partitioning of an image into finite, non-overlapping regions such that the pixels in each region share similar attributes [8, 9]. In quantitative studies, the information from segmentation can be used to analyze and measure tumor growth, and its response to treatments such as chemotherapy and radiation therapy [10, 11]. Software packages like OsiriX [12] allow doctors to view the entire brain volume as several image slices. However, there are still instances where, to determine the tumor volume, tumors must be detected manually and its boundaries traced by the doctors on each slice of the MRI sequence. This poses many difficulties as mentioned.

Several techniques for segmentation have been suggested. The simplest is thresholding. This separates an image into foreground and background by comparing pixel intensities to a threshold value [13]. Otsu [14] presented a method to determine the optimum thresholding value based on the image's grey-level histogram. Still, using thresholding to segment brain tumors can be difficult since tumors may have a grey-level coinciding with healthy brain tissue [1]. Another technique called region growing starts with a seed that belongs to the structure of interest and extracts all connected pixels that are similar [13]. Some disadvantages are that region growing requires human interaction for seed selection, and is noise sensitive [15]. Alternatively, clustering techniques classify pixels into a fixed number of clusters such that pixels in a cluster are similar but dissimilar to those in other clusters. Two common forms of clustering utilized are k-means and fuzzy c-means. In k-means, each pixel belongs to only one cluster whereas in fuzzy c-means, a pixel can belong to two or more clusters [8]. K-means is fast and simple, but results may vary as they depend on randomly selected initial centroids [5]. Fuzzy c-means is time consuming [1]. Furthermore, a comparison done in [8] found k-means to outperform fuzzy c-means in completeness of segmentation while maintaining outstanding correctness. Based on this previous analysis, k-means clustering was employed in the proposed work. Although there are many other techniques that may produce results with greater accuracy, computational complexity would be sacrificed [1].

This paper presents a novel, fully automatic brain tumor segmentation and volume estimation method using two types of MRI sequences: T1-contrasted and T2. Clinically, multiple MRI sequences are used to identify different compartments of the tumor [13]. Since using a combination of MRI sequences provides more information, it is inferred that the efficiency of an algorithm to define the boundaries can be increased. The brightness of the tumor border is enhanced in T1-contrasted images and likewise, the core and edema regions from the T2 image [13]. The algorithm combines these characteristic features from each image using a variety of techniques including anisotropic diffusion, k-means clustering, morphological operations, and temporal smoothing. From the segmentation, the volume of the tumor region is obtained by taking the sum of its voxels (pixel and thickness of MRI slice). This paper is organized as follows. Section 2 gives details of the proposed algorithm. Section 3 presents results of tests performed. Discussions are made in section 4, and conclusions in section 5.

2. METHODOLOGY

This section describes the proposed algorithm, whose respective flow chart is shown in Figure 1. The proposed work was implemented in the MATLAB environment, which contained numerous
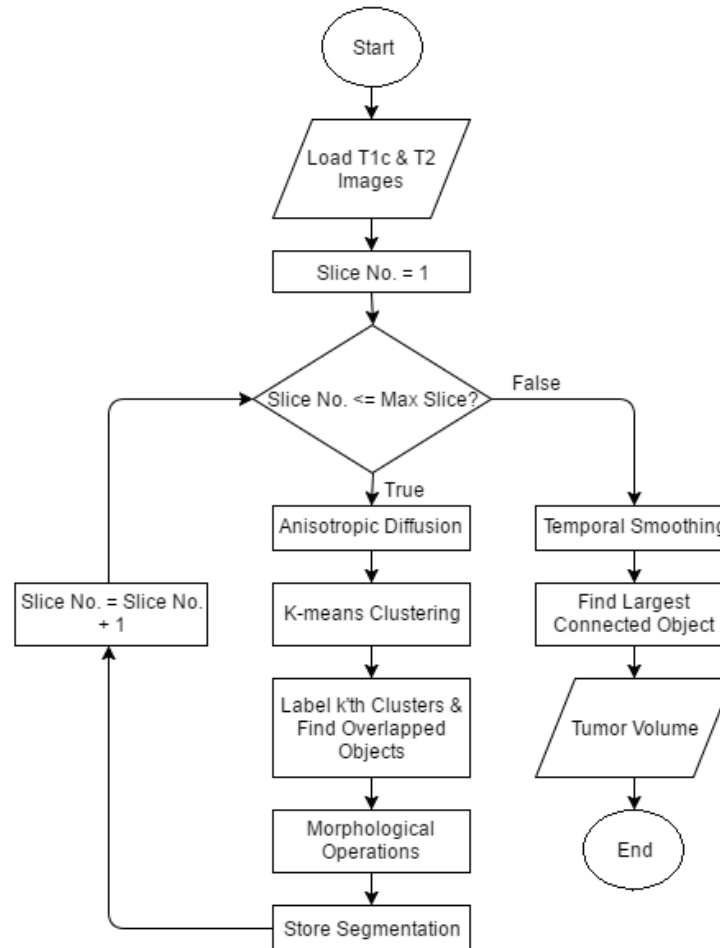
FIGURE 1: Flow chart of the proposed brain tumor segmentation and volume estimation algorithm.

image processing tools. The algorithm first loaded all the brain MRI slices (the volume) from the T1-contrasted and T2 scans. The dimensions of the MRI volumes were determined and two empty arrays of the same dimensions were created to store the results of the subsequent steps. The proposed segmentation procedure involved the use of: anisotropic diffusion, k-means clustering, combining overlapping regions, and morphological operations. The steps were performed on all corresponding slices from each sequence, then a temporal smoothing procedure was applied. This temporal smoothing procedure is a form of error checking that involved examining the consistency of the detected objects within a two-frame radius of the respective frame. Finally, the largest connected object segmented was selected as the tumor region, and its volume was found by summing its respective voxels. The preprocessing, segmentation and post-processing steps are explained further in the subsections below.

2.1 Anisotropic Diffusion
The preprocessing step improves upon the image quality to be more suitable for the segmentation step. Anisotropic diffusion filtering, proposed in [16] was used to eliminate noise in the image. It has an advantage over linear filters by smoothing the image without removing the edge information. The performance of this filter depends on several parameters: the conductance function, gradient magnitude threshold and the stopping time. The conductance function allows maximum diffusion within uniform regions and stops diffusion across edges. The gradient magnitude threshold controls the rate of diffusion and is a soft threshold between gradients attributed to noise and edges. Anisotropic diffusion is an iterative process. The choice of stopping
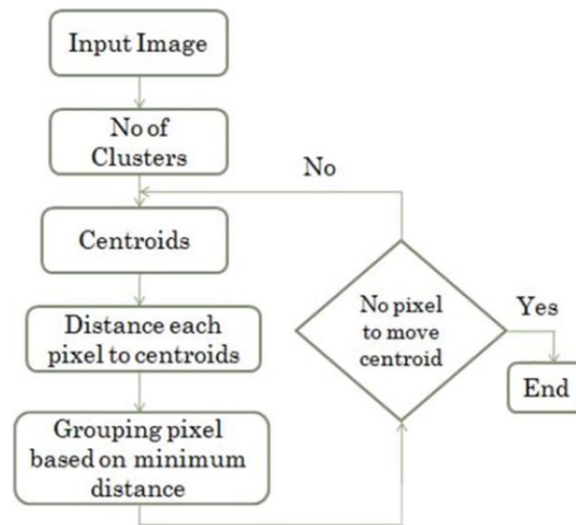
FIGURE 2: Flowchart of the k-means clustering algorithm [9]

time has significant impact, where overestimating this value will blur edges, and underestimating it will leave unfiltered noise [17]. In this work, a conductance function that favored high-contrast edges over low-contrast edges was selected. After preliminary tests on sample data sets, a gradient threshold of 7 and a 15-iteration stopping time were chosen. Figure 3 (a, d) illustrates the T1-contrasted and T2 images before filtering while figure 3 (b, e) illustrates after anisotropic diffusion was applied respectively.

2.2   K-Means Clustering

The segmentation step began with K-means, which is an unsupervised clustering algorithm. This means that no previously labeled examples are needed to find structure in the data [15]. The algorithm separates the intensity values in the image into k clusters. Initially, k centroids C_{1-k} are selected at random, where C_i (the i'th cluster) is within the intensity range of a grayscale image, 0-255. The distances of each pixel intensity in the image to each centroid is calculated. The pixel intensities are assigned to the centroid with the smallest distance. A new centroid is computed by finding the average of the distances of the assigned pixel intensities. The distances are recalculated using the new centroids and the pixels are reassigned. The cycle repeats until there are no changes in centroids or until a fixed number of iterations have been completed [1]. Figure 2 outlines the k-means algorithm.

Brain images encompass the white matter, grey matter, cerebrospinal fluid (CSF) and background [11]. This work also included the tumor as a separate class. The T1-contrasted image was divided into 4 clusters to classify the background and CSF together, grey matter, white matter, and tumor. The T2 image was divided into 5 clusters; the background and CSF were separated. The background and CSF were grouped as a single class in the T1-contrasted image due to the closeness of pixel intensities. Since information in this class was not used further, it was not a concern that the background and CSF were grouped. A maximum iteration of 25 was used. The k'th clusters were the most useful since the bright tumor pixels would be assigned to them. Figure 3 (c, f) shows the pixels assigned to the k'th clusters for the T1-contrasted and T2 images respectively.

2.3   Combining Overlapped Objects

The segmentation step continued by combining the information from k'th clusters and eliminating the noisy regions. MATLAB's *bwlabel* function was used to label the objects in the k'th cluster from each MRI sequence. The combination was accomplished by first performing a logical AND operation on the k'th clusters to identify the overlapping regions between the two images, shown in figure 3 (g).
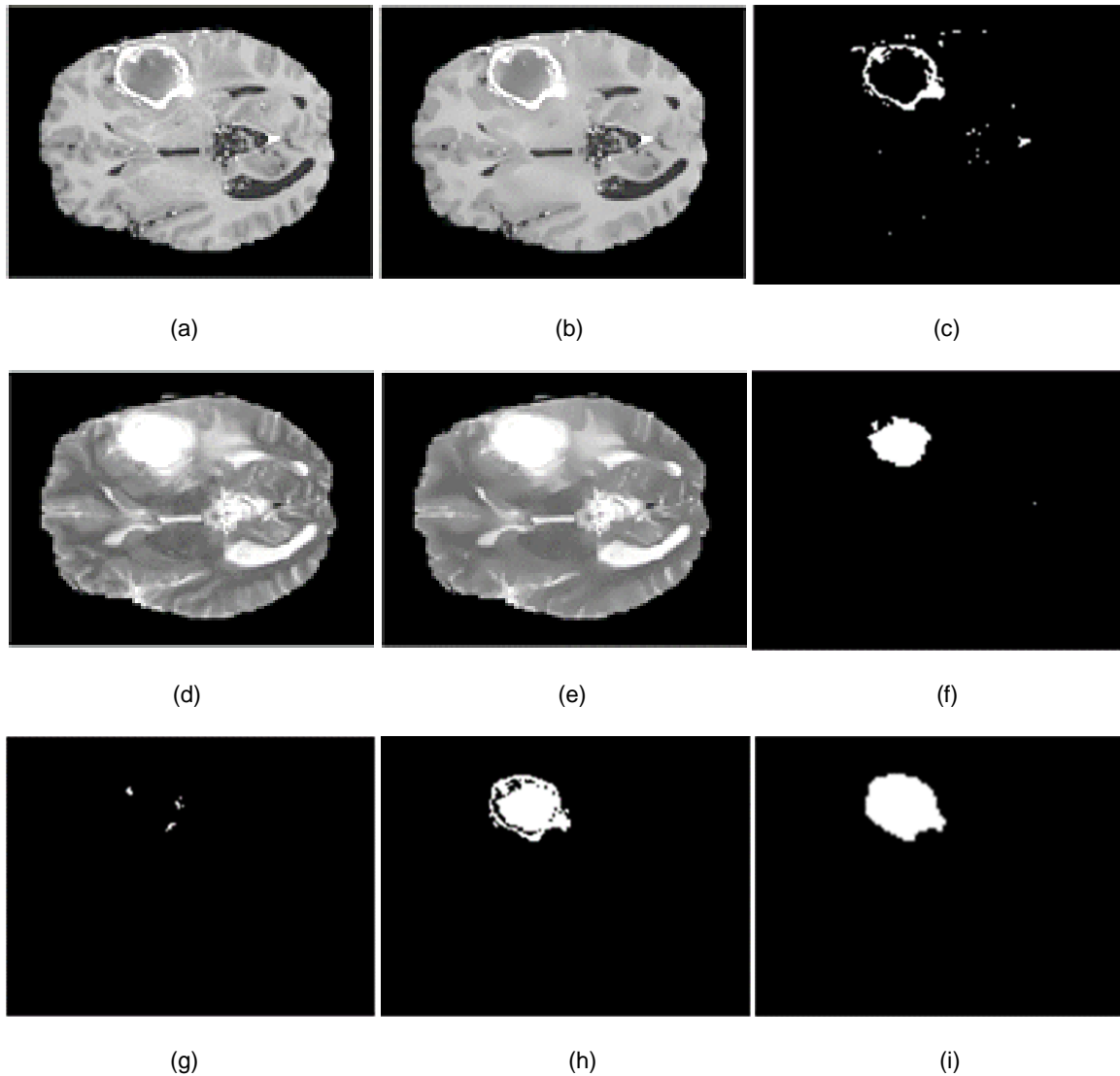
FIGURE 3: Major steps involved in the proposed segmentation algorithm. (a) T1-contrasted. (b) Filtered T1-contrasted. (c) T1-contrasted cluster 4. (d) T2. (e) Filtered T2. (f) T2 cluster 5. (g) Logical AND. (h) Combined segmented tumor (i) Post morphological operations (Closing, Erosion, Dilation).

Using the labelled images for each sequence, only the labels that belonged in the overlap were extracted, and new images were generated displaying objects having the selected labels. These images were added together to give the segmented tumor image in figure 3 (h). It can be seen that the noisy pixels from figure 3 (c, f) were eliminated.

2.4 Morphology

Post-processing steps were taken to further improve the accuracy of the segmented tumor regions using morphological operations in the order of closing, erosion and dilation. This filled any holes in the tumor regions and smooths the edges. These operations were done using MATLAB's *imfill*, *imerode* and *imdilate* functions. A 3x3 structuring element was used. The morphological operations are mathematically described below in equations (1), (2), and (3) respectfully. Figure 3 (i) shows the result generated in this step using the image in figure 3 (h).

Morphological closing of a binary image A by a structuring element B [11]

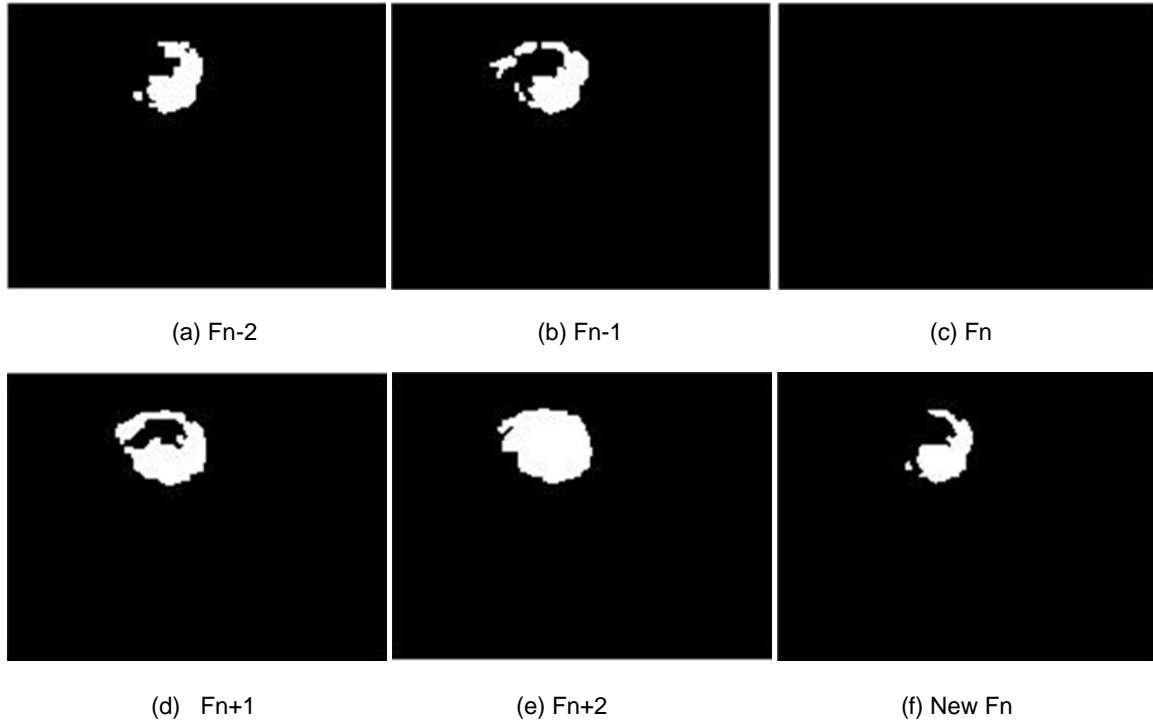$$A \bullet B = (A \oplus B) \ominus B \qquad (1)$$

(a) Fn-2 (b) Fn-1 (c) Fn

(d) Fn+1 (e) Fn+2 (f) New Fn

FIGURE 4: Temporal smoothing applied on a frame Fn. After segmentation, frame Fn in (c) was erroneous in that it contained no objects while its neighboring frames did, as shown in (a, b, d, e). This error was rectified by using a weighting scheme in a five-frame window to produce (f).

Morphological erosion of a binary image A by a structuring element B [4]

$$A \ominus B = \{z | (B)_z \subseteq A\} \qquad (2)$$

Morphological dilation of a binary image A by a structuring element B [4]

$$A \oplus B = \{z \,|\, (B^-)\_z \cap A \neq \Phi\} \qquad (3)$$

2.5   Temporal Smoothing

Once the previous steps have been completed for all slices and the result stored in the first empty array, temporal smoothing was performed to maintain consistency throughout the segmentations obtained. The first and last two segmented image slices were copied to the second empty array, which stores the result of the temporal smoothing. In this procedure segmentations for a frame, F_n (where n = 3: max. slice − 2), were obtained using a weighted average scheme from a five-frame sliding window, as described in equations (4) and (5). The result from each frame was cleaned using a median filter. Figure 4 shows sample images that were generated in this step for a frame Fn before and after temporal smoothing.

$$F_n \; = \; 0.1F_{n-2} + \; 0.2 \, F_{n-1} + \; 0.4F_n \; + \; 0.2F_{n+1} \; + \; 0.1F_{n+2} \qquad (4)$$

$$F_n \; = \; F_n > 0.5 \qquad (5)$$

2.6   Find the Largest Connected Object

MATLAB's *bwlabeln* function was used to label connected objects throughout the segmented volume; that is the second array. The properties of the connected components were measured and the largest object label was determined. The tumor was considered the largest object. The sum of all pixels that made up the tumor was taken and multiplied by the voxel dimensions (given in the MRI sequence) to find the tumor volume.
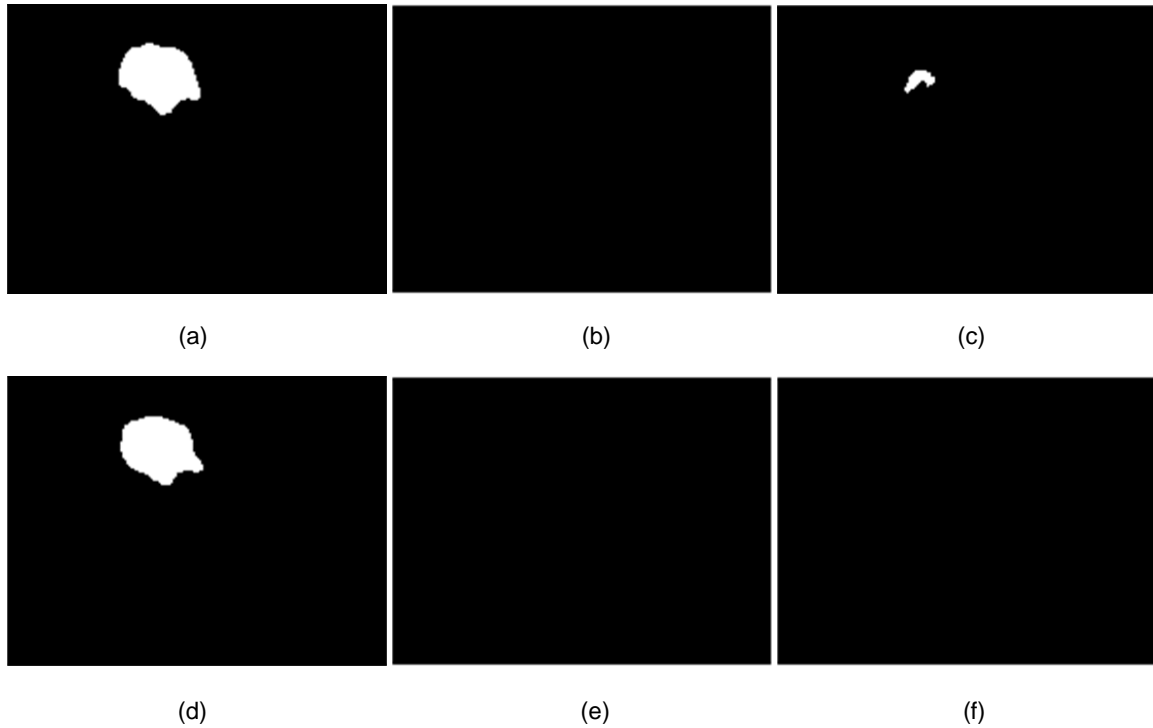
FIGURE 5: Sample Segmentation results of three test cases by the proposed algorithm. Tumor ground truth frames are shown in (a), (b) and (c) and the corresponding segmentations obtained where the tumor regions were: (d) correctly identified, (e) correctly not detected, and (f) not detected.

3. RESULTS

The algorithm was tested using brain volumes from the MICCAI BRATS 2012 dataset [18]. This dataset consisted of T1, T1-contrasted, T2 and Flair MRI sequences. Ground truth data was also provided, and all images were skull-stripped and aligned. In each test case, a voxel size was 1mm x 1mm x 1mm. The precision, recall, specificity and Dice Score Coefficient (DSC) metrics were used to evaluate the tumor regions obtained. Precision is a measure of accuracy, recall is a measure of completeness, and specificity measures the true negative rate. The DSC measures the overlap between the ground truth and the automatic segmentation. The calculation of these metrics is given in equations (6) through (9) respectfully.

$$Precision = \frac{TP}{(TP+FP)} \times 100\%$$

(6)

$$Recall = \frac{TP}{(TP+FN)} \times 100\%$$

(7)

$$Specificity = \frac{TN}{(TN+FP)} \times 100\%$$

(8)

$$DSC = \frac{2TP}{(FP+2TP+FN)}$$

(9)

Where: TP – True Positive; TN – True Negative; FP – False Positive; FN – False Negative

A true positive was counted for every pixel in the detected tumor region having a binary 1 value that matched the ground truth. A false positive was counted for every pixel in the detected tumor region that had a binary 1 value, but the corresponding pixel in the ground truth had a binary 0 value. A true negative was counted for every pixel in the detected tumor region having a binary 0
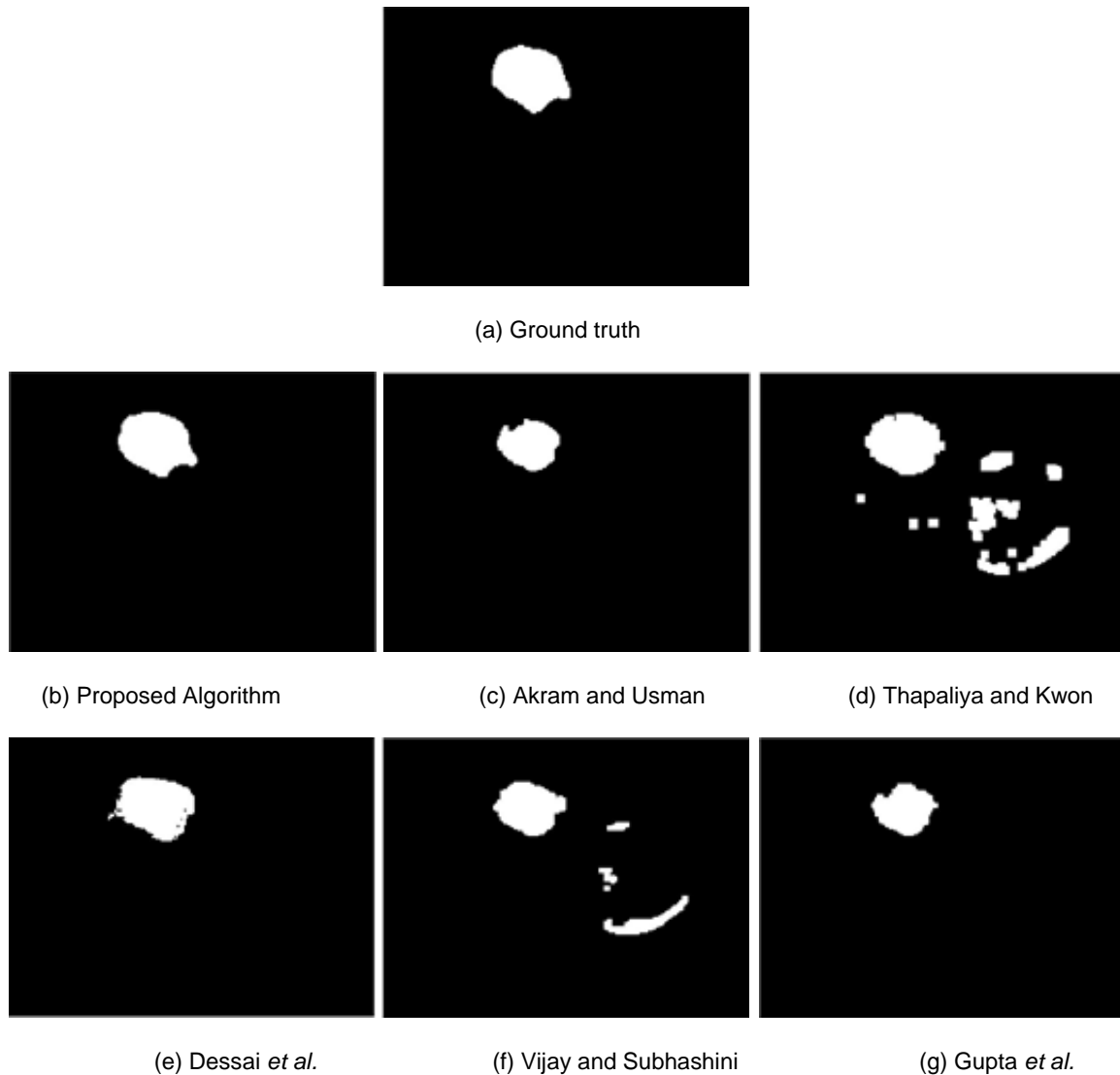
(a) Ground truth

(b) Proposed Algorithm   (c) Akram and Usman   (d) Thapaliya and Kwon

(e) Dessai *et al.*   (f) Vijay and Subhashini   (g) Gupta *et al.*

FIGURE 6: Brain tumor single-slice sample segmentations detected by algorithms examined. (a) Ground truth. (b) Proposed algorithm. (c) Akram and Usman [4]. (d) Thapaliya and Kwon [5]. (e) Dessai *et al.* [1]. (f) Vijay and Subhashini [9]. (g) Gupta *et al.* [19].

value that matched the ground truth. Lastly, a false negative was counted for every pixel in the detected tumor region that had a binary 0 value, but the corresponding pixel in the ground truth had a binary 1 value. Figure 5 shows samples of the detected tumor regions by the proposed algorithm compared to the ground truth. These samples include three cases where the tumor region was: correctly identified, correctly not detected for a non-tumor slice, and not detected.

The algorithm was compared to several others in previous works [1, 4, 5, 9, 19]. To obtain the tumor region, thresholding and morphological operations were used by three authors: Akram and Usman [4], Thapalya and Kwon [5], and Gupta *et al.* [19], while k-means was used by two authors: Dessai *et al.* [1], and Vijay and Subhashini [9]. They were all fully-automatic and used one MRI sequence, T2, except for Gupta *et al.* [19], which was semi-automatic and used three MRI sequences, T1 and T1-contrasted included. The tests were conducted on 20 brain volumes. The quality of the images in each test volume varied, often having less contrast or tumor regions that were indistinguishable by an untrained eye. These variations in image quality caused high fluctuations in values obtained from all algorithms. Figure 6 shows sample tumor outputs for one
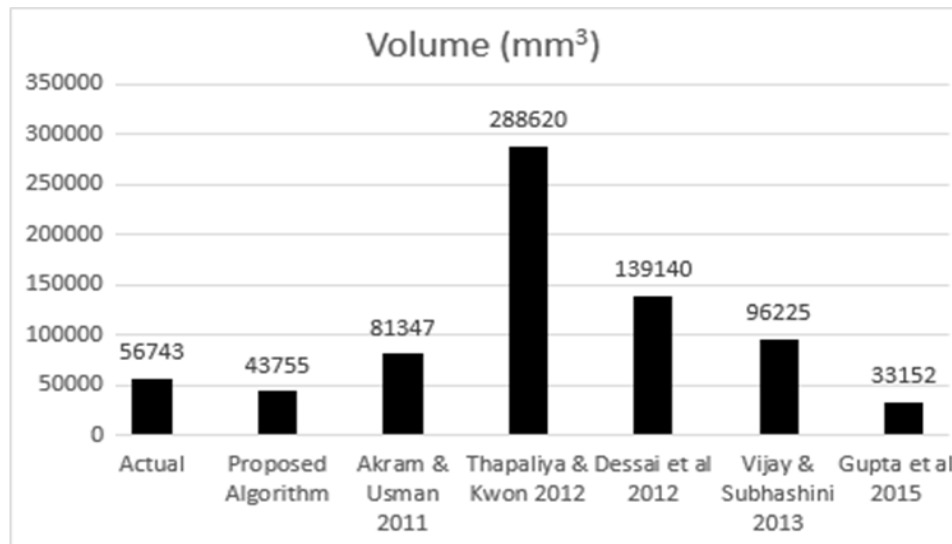
FIGURE 7: Tumor volumes obtained from the first test sequence for all algorithms examined.

MRI slice in the first test volume, detected by all algorithms examined. Figure 6 (a) is the expertly segmented ground truth to which the results from the algorithms were compared. In this instance, the proposed algorithm produced a tumor region visibly similar in size and shape to the ground truth, shown in figure 6 (b). This can be attributed to combination of T1-contrasted and T2 tumor boundaries. Other algorithms reasonably identified the region of interest with the tumor area less or greater than the ground truth. Though, Thapalya and Kwon [5] and Vijay and Subhashini [9] in figure 6 (d, f) respectively, also detected sizable false positives.

Results for the experiments with regards to the average tumor volume, precision, recall, specificity, and DSC values obtained from each algorithm are given in figures 7-11 respectively. Figure 7 shows the volumetric measurements of the tumor regions obtained by the different algorithms from the first test case. The actual tumor volume, which was taken as the sum of all tumor pixels in the ground truth, was 56743 mm^3. The proposed algorithm measured less volume than the actual tumor at 43755 mm^3. Still, this was the closest value to the actual, having a difference of 12988 mm^3 or an absolute error of 22.89%. The percentage absolute error values obtained from the past algorithms in increasing order are as follows: 41.58% from Gupta *et al.* [19], 43.36% from Akram and Usman [4], 69.58% from Vijay and Subhashini [9], 145.21% from Dessai *et al.* [1], and 408.64% from Thapalya and Kwon [5]. Gupta *et al.* [19] measured the lowest volume of 33152 mm^3. The other algorithms had a volume greater than the actual due to a high number of false positives detected.

In the first test case, the proposed algorithm recorded the highest precision value of 88.55%, a minor lead over Gupta *et al.* [19] with 85.09%. Next was Akram and Usman's [4] algorithm at a precision of 69.85%. This was closely followed by Dessai *et al.* [1] with 69.49%. The algorithm by Vijay and Subhashini [9] had 66.57% precision, and the lowest was Thapaliya and Kwon [5] with 53.71%. Dessai *et al.* [1] had the most complete actual tumor with a recall of 81.47%. Thapaliya and Kwon [5] followed with 79.33%, then the proposed algorithm at 72.52%. Vijay and Subhashini's [9] algorithm had a recall of 64.03%. Lastly, Akram and Usman's [4] and Gupta *et al.* [19] detected half of the tumor with their 50.98% and 49.71% recall, respectively. In this test case, the proposed algorithm determined that no tumors existed in all the non-tumor slices as shown by its specificity value of 100%. All algorithms performed similarly well in this area with the lowest specificity value being 95.91% from Thapaliya and Kwon [5]. The DSC gave a value between 0 and 1, where 1 represented perfect overlap. These values closely followed that of the recall.

Despite the inconsistency of image quality, the proposed algorithm outperformed others where the highest precision value was recorded in 45% of the test cases. Since the recall values were frequently lower than the corresponding precision values unlike other algorithms, the tumor volume would have been made up more of the actual tumor than false positives. The DSC reflected the recall. The proposed algorithm was also able to confirm non-tumor slices better than the other algorithms, as seen from the specificity values.
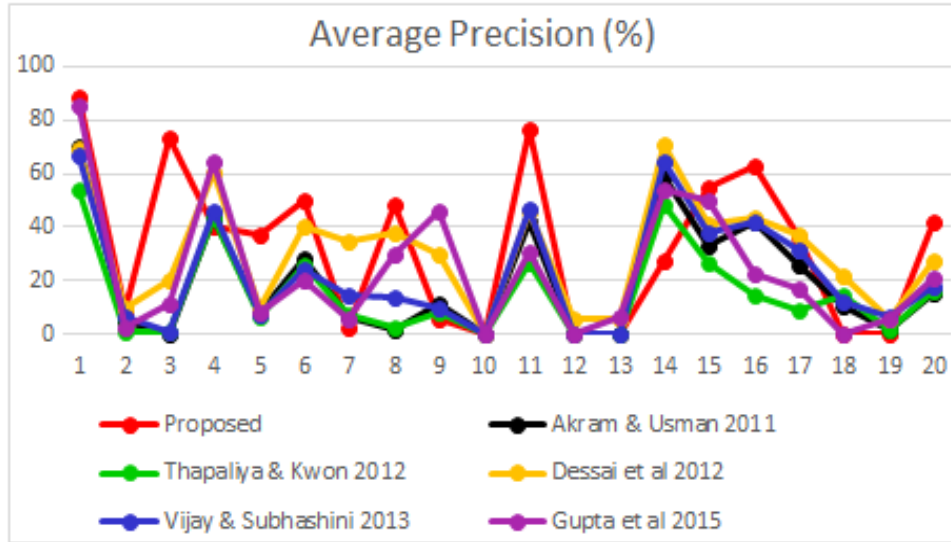

FIGURE 8: Average precision values obtained from all algorithms examined for 20 test volumes.
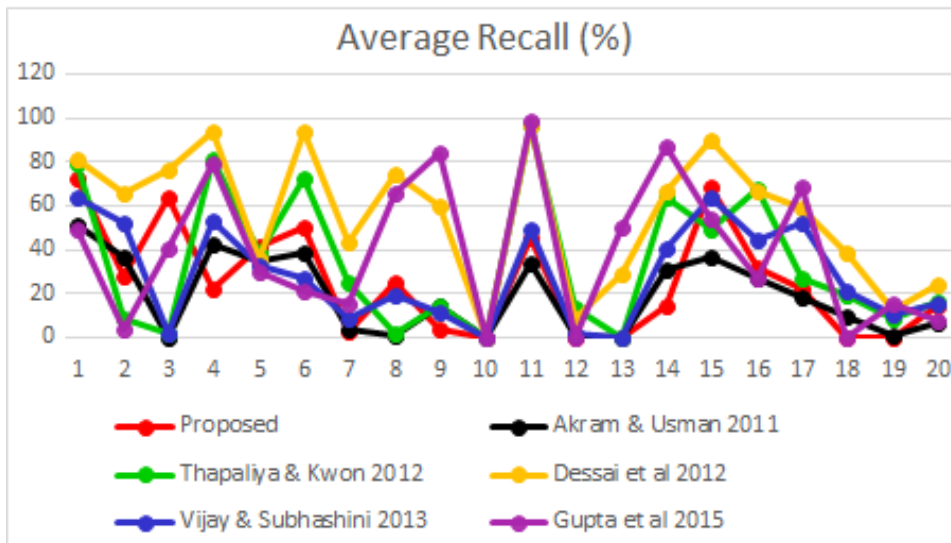

FIGURE 9: Average recall values obtained from all algorithms examined for 20 test volumes.
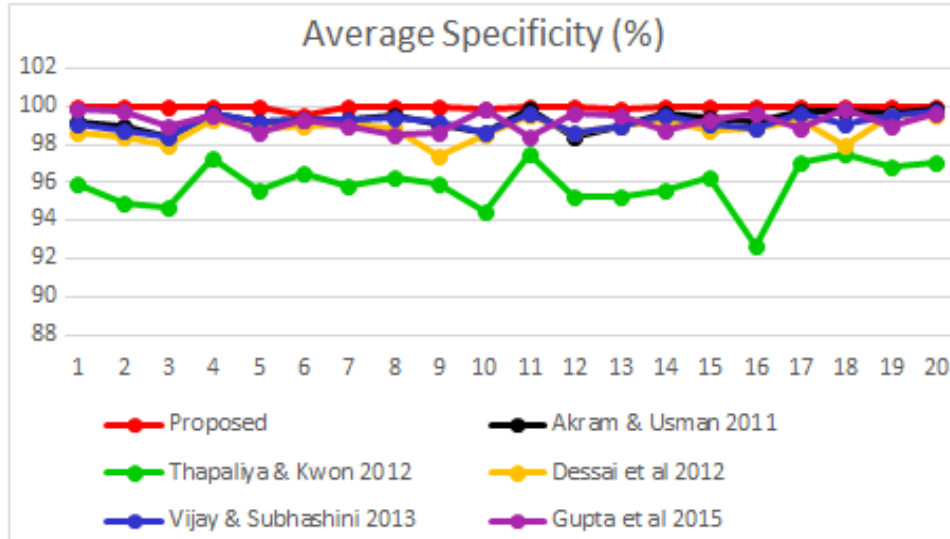
FIGURE 10: Average specificity values obtained from all algorithms examined for 20 test volumes.
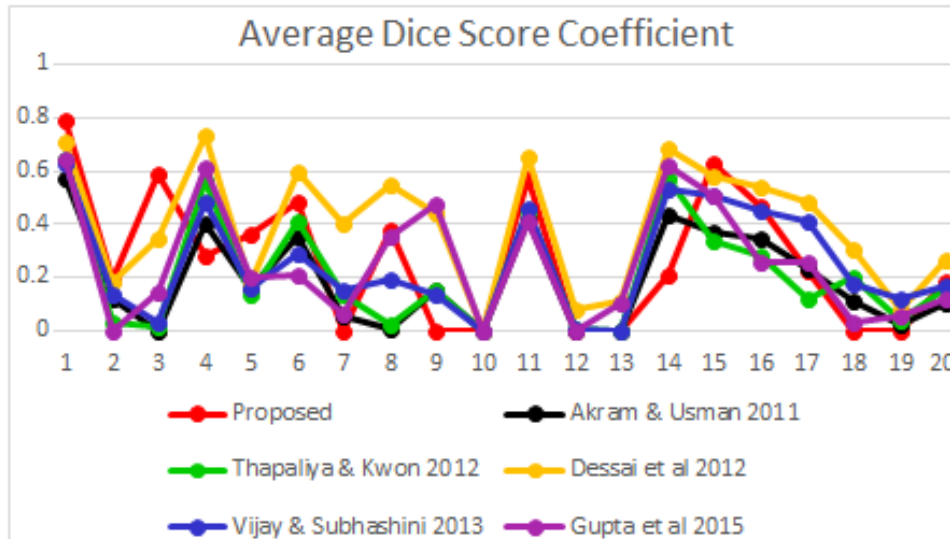

FIGURE 11: Average DSC values obtained from all algorithms examined for 20 test sequences.

4. DISCUSSION

Precision and recall values can give a sense of the tumor volume output and its closeness to the actual. Ideally, it is desirable for both the precision and recall values to be high. This would mean that there were little to no false positives and the actual tumor pixels were almost entirely detected. A low precision means many false positives were detected which would increase the volume output of the tumor. If the corresponding recall was high, a lot of the actual tumor made up that volume, but if it was low, then the actual tumor made up less of that volume. In the comparison of algorithms for the first test volume, the proposed algorithm had the highest accuracy, and lower recall. While the algorithm by Dessai *et al.* [1] had a recall higher than the proposed algorithm, their precision value was even lower. It is more favorable to have a precision value higher than the recall value as opposed to a recall value higher than the precision value. Less of the actual tumor may have been detected but there would be little false positives, instead of having more of the actual tumor along with greater false positives representing healthy brain tissue. This is supported by the volume measurements where the proposed algorithm had

produced a volume less than the actual tumor with the smallest error. The algorithms by Dessai *et al.* [1], and Thapaliya and Kwon [5] produced the two highest volumes with great error from the actual.

Certain steps taken by past algorithms intended to improve performance may have had the opposite effect. Contrast enhancement is widely used as a preprocessing step to make the tumor more distinguishable. This makes the bright tumor pixels brighter and the dark, healthy brain tissue darker. The algorithms would identify the bright pixels as the tumor. While contrast enhancement works great for tumor slices, when it is performed on non-tumor slices it increases the intensity of the healthy brain tissues. Since the algorithms segment the bright pixels as the tumor, false positives would increase. For this reason, contrast enhancement was not used in the proposed algorithm. After thresholding or clustering was done, some algorithms selected the object with the largest area in a slice as the tumor region, eliminating others as noise. The issue with this is that there may be bright non-tumor regions or noise segmented that are larger than the tumor. Therefore, when selecting the largest connected object in that slice, false positives would be selected. By using two MRI sequences in the proposed algorithm, finding the overlap confirmed tumor regions and eliminated noise in the images. Instead of selecting the object with the largest area in each slice, the object with the largest volume throughout all slices was taken as the tumor. An inference made was that superior results can be obtained when information from the T1-contrasted and T2 MR Images are combined. Evidence of this claim was seen when the algorithm by Gupta *et al.* [19], which used T1, T1-contrasted and T2 MR Images, obtained the best results among the authors who utilized thresholding and morphological operations to obtain the tumor region. However, it should be noted that this algorithm was semi-automatic where a rough outline of the tumor region was manually identified, possibly improving tumor detection and eliminating noise.

The proposed algorithm had shortcomings of its own. The use of k-means clustering had random initial centroids selected. Testing the same brain volume again may produce slightly different results as the initial centroids would affect the outcome of clustering. It was suggested in [20] that it is better if the centroids are as far apart as possible. Since a grayscale image has a range of 0-255 intensity and the number of clusters is known, fixed centroids can be found that are an equal distance apart. The centroid at the high end of the intensity range would be of interest as the bright tumor would be assigned to it. However, the use of fixed centroids would not be advisable if the image quality is not consistent, as with the dataset used. If the contrast is low or the tumor shares intensity with healthy brain tissue, then no pixels would be assigned to the interested centroid leading to false negatives. Another possible problem is that the bright clusters from any slice of the T1-contrasted and T2 images may not overlap, suggesting that there is no tumor in that slice and leading to false negatives. This was solved by temporal smoothing, where data from slices before and after were used to fill any gaps. Lastly, the execution time taken for the proposed algorithm was longer than others. This occurred for several reasons: the steps used were applied to two MRI sequences instead of one, as well as the added time taken for iterations in anisotropic diffusion and k-means clustering.

The different procedures utilized in the proposed algorithm allowed for improvements from those in past works. Anisotropic diffusion sufficiently enhanced the images while preserving the edge information needed to delineate tumor boundaries. Since contrast enhancement was not done, the proposed algorithm saw a reduction of false positives detected in healthy brain MRI slices. This kept the volume output from the proposed algorithm closer to the actual volume while algorithms that used contrast enhancement saw a significant increase. In the segmentation phase, k-means clustering effectively classified the regions of the brain better than simply thresholding. Here, healthy brain tissue with intensities appearing similarly to the tumor region was less likely to be falsely identified. The reiterated centroids in k-means allowed the regions of the brain to be classified despite the images sometimes having low contrast. This is not possible using thresholding since the threshold value is fixed. The past algorithms examined that used k-means only applied this technique on one MRI sequence. By using two MRI sequences in the proposed algorithm, tumor boundaries that may not have been visible in one MRI sequence were

able to be recognized in the other. When the objects detected were labelled and the overlap found, the proposed algorithm could automatically identify and confirm the region of interest as well as effectively remove noisy objects. Manual intervention was not needed. The addition of information from the two MRI sequences resulted in a more complete tumor. Furthermore, morphological operations were also used by past algorithms in their post-processing phase. This filled in any holes and smooths the edges of segmentations in a MRI slice. Nevertheless, for a tumor slice where no tumor was detected, this step offered no assistance in filling in gaps. The proposed algorithm implemented temporal smoothing which catered to this scenario given that tumors were detected in neighboring slices. Segmentation gaps that occurred in MRI slices were filled in and noise was also reduced by the weighted-average scheme, essentially improving true positive detection and reducing false positives. Lastly, the proposed algorithm selected the largest object volume as the tumor. This possibly reduces false positive regions selected unlike past algorithms which would have selected the largest area per slice. Selecting the largest area per slice may have wrongfully selected noisy regions instead of the tumor, reducing the precision of the algorithm to detect the tumor.

The algorithms were all compared on the same dataset and measured with metrics commonly used for evaluation in past works, such as precision and recall [21]. The favorability of high precision and recall, or higher precision over recall was discussed with respect to what the values indicate about the tumor volume detected. The proposed algorithm achieved the highest precision in 45% of the test volumes that is more times than any other algorithm examined. Every step in the proposed algorithm saw attempts to improve the image quality and region of interest extraction, reduce noise, and fix errors in the segmentation results, to increase the precision and recall. The discussion on steps taken in this work illustrates the impact that can make in tumor detection. In the future, as techniques continue to advance and are reviewed [22], segmentation methods that are faster and more effective can be adopted. The method used for combining data from T1-contrasted and T2 MR images can also be refined for cases where no overlapped between the images were found, although this issue was fixed by implementing temporal smoothing. Pre-processing steps can be added for images that are not skull-stripped or aligned. Tests can also be repeated on datasets where the image quality is consistent. Other works include adding options allowing users to make manual interventions in selecting the region of interest, as well as applying the techniques used in the proposed work on the T2 MRI if the T1-contrasted MRI is not available. Tests would need to be carried out to validate the effectiveness of applying the techniques used in the proposed work on the T2 MRI only. The suggested actions would guarantee that the most is made of the work.

5. CONCLUSION
Brain tumors are the most prevalent cause of cancer-related deaths in young people [23], and to diagnose and treat the deadly disease effectively, analysis of hundreds of MRI scans is usually performed manually. This manual procedure is not only very tedious and time-consuming for doctors, but also error prone. This paper presented a new, simple technique to automatically segment brain tumors from a combination of T1-contrasted and T2 MRIs, and obtain their volumes. Steps taken include anisotropic diffusion, k-means clustering, morphological operations and temporal smoothing. The algorithm was tested on 20 brain volumes with over 100 slices each from the MICCAI BRATS 2012 dataset, and compared to several others in previous works. Its performance was measured using the precision, recall, specificity and DSC metrics. From the results, the proposed algorithm outperformed those in past works. It is noted that none of the algorithms obtained consistent results; this was probably due to the large variance in image quality among the data set. Despite the poor image quality however, the proposed algorithm outperformed others in the category of precision, obtaining the highest precision values in 45% of the test cases. Advances were seen by its noise reduction, increase in accuracy and closeness to actual tumor volume. Future works include adopting more sophisticated segmentation techniques, making improvements to reduce the execution time, and adjusting the algorithm to cater for data that is not skull-stripped or aligned. Additionally, an alternate, semi-automatic option can be included to allow users to draw a region of interest for segmentation on the MRI. Should

T1-contrasted MRIs not be available, users can also have the choice to apply steps taken on the T2 MRI sequence only. These measures would ensure that users benefit from this work.

6. REFERENCES

[1]   V. S. Dessai, M. P. Arakeri and G. R. M. Reddy, "A parallel segmentation of brain tumor from magnetic resonance images," in ICCCNT, 2012, pp. 1-6.

[2]   Bhattacharjee and M. Chakraborty, "Brain tumor detection from MR images: Image processing, slicing and PCA based reconstruction," in EAIT, 2012, pp. 97-101.

[3]   T. S. D. Murthy and G. Sadashivappa, "Brain tumor segmentation using thresholding, morphological operations and extraction of features of tumor," in ICAECC, 2014, pp. 1-6.

[4]   M. U. Akram and A. Usman, "Computer aided system for brain tumor detection and segmentation," in ICCNIT, 2011, pp. 299-302.

[5]   K. Thapaliya and G. R. Kwon, "Extraction of brain tumor based on morphological operations," in ICCM, 2012, pp. 515-520.

[6]   World Health Organization. "Cancer." Internet: www.who.int/mediacentre/factsheets/fs297-/en/, Feb., 05, 2016 [Jan., 25, 2018].

[7]   A. A. Siddiqi, A. Khawaja and M. Tariq, "3D volume representation of brain tumor using Image Processing," in ICSIPA, 2011, pp. 75-75.

[8]   G. M. N. R. Gajanayake, R. D. Yapa, and B. Hewawithana, "Comparison of standard image segmentation methods for segmentation of brain tumors from 2D MR images." in ICIIS, 2009, pp. 301-305.

[9]   J. Vijay and J. Subhashini, "An efficient brain tumor detection methodology using K-means clustering algorithm," in ICCSP, 2013, pp. 653-657.

[10] X. Li, S. Lebonvallet, T. Qiu and S. Ruan, "An improved level set method for automatically volume measure: application in tumor tracking from MRI images," in EMBS, 2007, pp. 808-811.

[11] M. P. Beham and A. B. Gurulakshmi, "Morphological image processing approach on the detection of tumor and cancer cells," in ICDCS, 2012, pp. 350-354.

[12] The OsiriX Development Team. "OsiriX Imaging Software 2010." Internet: http://www.osirix-viewer.com/, Jan. 1, 2010 [Jan., 25, 2018].

[13] J. Liu, M. Li, J. Wang, F. Wu, T. Liu and Y. Pan. (2014, Dec.). "A survey of MRI-based brain tumor segmentation methods." Tsinghua Science and Technology. [Online]. 19 (6), pp. 578-595. Available: 10.1109/TST.2014.6961028

[14] N. Otsu. (1979, Jan.). "A threshold selection method from gray-level histograms." IEEE transactions on systems, man, and cybernetics. [Online]. 9(1), pp. 62-66. Available: http://web-ext.u-aizu.ac.jp/course/bmclass/documents/otsu1979.kpdf

[15] M. M. Ahmed and D. B. Mohamad. (2008, Feb.). "Segmentation of brain MR images for tumor extraction by combining kmeans clustering and perona-malik anisotropic diffusion model." International Journal of Image Processing. [Online]. 2 (1), pp. 27-34. Available: http://www.cscjournals.org/manuscript/Journals/IJIP/Volume2/Issue1/IJIP-8.pdf

[16] P. Perona and J. Malik. (1990, Jul.). "Scale-space and edge detection using anisotropic diffusion." IEEE Transactions on Pattern Analysis and Machine Intelligence. [Online]. 12 (7), pp. 629-639. Available: http://authors.library.caltech.edu/6498/1/PERieeetpami90.pdf

[17] C. Tsiotsios and M. Petrou. (2013, May). "On the choice of the parameters for anisotropic diffusion in image processing." Pattern recognition. [Online]. 46 (5), pp. 1369-1381. Available:
https://pdfs.semanticscholar.org/6d18/674b370247dc7ffc9ec6bf3cd808bc794eb2.pdf

[18] B. H. Menze, A. Jakab, S. Bauer, K. Farahani, J. Kirby, Y. Burren, N. Porz, J. Slotboom, R. Wiest and L. Lanczi. (2015, Oct.). "The multimodal brain tumor image segmentation benchmark (BRATS)." IEEE transactions on medical imaging. [Online]. 34(10), pp. 1993-2024. Available: http://ieeexplore.ieee.org/stamp/stamp.jsp?arnumber=6975210

[19] M. Gupta, B.P. Rao, V. Rajagopalan, A. Das, and C. Kesavadas, "Volumetric segmentation of brain tumor based on intensity features of multimodality magnetic resonance imaging," in IC4, 2015, pp. 1-6.

[20] M. M. Hossam, A. E. Hassanien, and M. Shoman, "3D brain tumor segmentation scheme using K-mean clustering and connected component labeling algorithms," in ISDA, 2010, pp. 320-324.

[21] M. A. Qadar and Y. Zhaowen. (2014, Nov.). "Brain Tumor Segmentation: A Comparative Analysis." International Journal of Computer Science Issues. [On-line]. 11(6), pp. 1694-0784. Available: https://arxiv.org/abs/1503.02466

[22] M. Angulakshmi and G. G. L. Priya. (2017, Mar.). "Automated brain tumour segmentation techniques— A review." International Journal of Imaging Systems and Technology. [On-line]. 27(1), pp. 66-77. doi:10.1002/ima.22211

[23] American Brain Tumor Association. "Malignant brain tumors most common cause of cancer deaths in adolescents and young adults: First comprehensive study of 15-39 year-old population." Internet: www.sciencedaily.com/releases/2016/02/160224132910.htm, Feb., 01, 2016 [Jan., 25, 2018].